Int. J. Heat Mass Transfer. Vol. 30, No. 3, pp. 581–588, 1987
Printed in Great Britain

0017–9310/87 $3.00 + 0.00

Flooding and hysteresis effects in nearly-horizontal countercurrent stratified steam–water flow†

S. G. BANKOFF
Chemical Engineering Department, Northwestern University, Evanston, IL 60201, U.S.A.

and

S. C. LEE

Mechanical Engineering Department, Yeungnam University, Gyongsan 632, Korea

(*Received* 17 *September* 1985 *and in final form* 11 *July* 1986)

Abstract—Experimental data are presented on flooding transitions, together with a countercurrent-flow regime map for nearly-horizontal ($\theta = 4.0$) stratified steam–water flow. The influence of condensation on the initiation and basic mechanisms of flooding is explored. The mechanism of hysteresis effects owing to condensation, which are observed during the partial delivery stage in a steam/subcooled water flow, are also investigated.

INTRODUCTION

IN RECENT years the flooding phenomenon has been extensively studied in connection with the safety analysis of nuclear reactor systems, but some features of flooding are still not thoroughly understood. For example, the exit and entrance geometries appear to be critical in determining both the vapor flooding velocity and the point of initiation of flooding. In steam–water flows the condensation effect not only alters the vapor flooding velocity but also changes the flow characteristics during the partial delivery stages. If flooding is initiated at some location other than the bottom of the tube the condensation effect tends to be significant. In this case the effective steam flow rate to initiate flooding, in which the overall condensation rate is subtracted from the steam supply rate, controls. Regardless of the initiation locus, this condensation effect can cause a sudden reduction of the liquid delivery rate once flooding starts. This bistable operating condition can lead to a hysteresis effect in cyclic operation. This has also been reported for non-condensing flows [1, 2], but the basic mechanisms are quite different.

Flooding in horizontal, or nearly-horizontal, stratified countercurrent flow, apart from its intrinsic scientific interest, may occur in several phases of small-break PWR accidents. This phenomenon is explored in the present study. The basic mechanisms of the hysteresis effects due to the breakup of liquid films, as well as condensation, are also discussed. Experimental data on flooding velocity, partial delivery rate, and critical vapor velocity, both in steam/saturated water flow and in steam/subcooled water flow, are presented. Finally, a countercurrent-flow regime map is constructed, which spans the transition from a stable operating region to completely cocurrent upward flow.

†Work supported by the U.S. Nuclear Regulatory Commission.

PREVIOUS WORK

Flooding correlations in a single channel flow have been, in general, described in terms of two dimensionless velocities, J^*, suggested by Wallis [3], representing the ratio of inertia force to hydrostatic force

$$J_k^* = j_k\left[\frac{\rho_k}{(\rho_f - \rho_g)gD}\right]^{1/2}, k = \text{g or f} \qquad (1)$$

where j_k is the superficial velocity of the k-phase and D is a length scale, taken to be the equivalent diameter. The length scale in J^* is simply replaced by the Laplace capillary length to obtain K, the Kutateladze parameter used by Tien [4]. Several J^* correlations have been proposed for the onset of flooding in vertical annular countercurrent flow [1, 5, 6] in the form given by Wallis [3]

$$J_g^{*1/2} + mJ_f^{*1/2} = C \qquad (2)$$

where m and C are empirical constants.

For inclined or nearly-horizontal stratified flow, Lee and Bankoff [7, 8] employed a modified J^*

$$J_{mk}^* = j_k\left[\frac{\rho_k}{gL\sin\theta(\rho_f - \rho_g)}\right]^{1/2} \qquad (3)$$

where L is the length scale, which is in general taken

NOMENCLATURE

C	empirical constant, equation (2)	m	empirical constant, equation (2).
C_{pl}	liquid specific heat		
D	equivalent diameter	Greek symbols	
f	condensation efficiency	ρ	density
g	acceleration due to gravity	θ	angle of inclination with the horizontal.
H	height (distance between top and bottom plates) of test section	Subscripts	
i_{fg}	latent heat of vaporization	e	effective
J^*	dimensionless velocity, equation (1)	f	liquid
j	superficial velocity	g	gas
Ja	modified Jakob number, equation (5)	in	inlet
K	Kutateladze number	k	kth (k = f or g)
L	length scale	m	modified
		s	saturation.

to be the hydraulic diameter of the test section. Therefore, L will be $2H$ for a rectangular channel and $L = H$ for a square duct. An envelope theory, which considers flooding to be the limiting condition for countercurrent flow, was developed to predict the onset of flooding for this flow. Their data, taken in a flow with relatively ideal entrance and exit conditions, were in good agreement with the theory. Wallis and Dobson [9] found that the gas flooding velocity for horizontal countercurrent flow is as little as half of that predicted by the Kelvin–Helmholtz stability theory. Later, Mishima and Ishii [10], following Kordyban and Ranov [11], developed a finite-amplitude theory, based on the fastest-growing interfacial wave, which can be modified to predict the onset of flooding in countercurrent flow [12]. These theories also appear to be in good agreement with the flooding data obtained under smooth entrance and exit conditions [7]. However, in most practical cases, the flooding velocity is expected to be substantially reduced because of maldistribution of the liquid film, as well as the presence of a hydraulic jump at the liquid entrance. These effects have been described in vertical annular countercurrent flow [13], but no quantitative description has yet been given for nearly-horizontal countercurrent flow.

For vertical condensing countercurrent flow, Block and Crowley [14] suggested that equation (2) remains valid, provided that the effective dimensionless steam flow rate, J^*_{ge}, is substituted for the dimensionless

$$J^*_{ge} = J^*_g - fJa\,J^*_{f,in} \tag{4}$$

where f is the condensation efficiency and Ja is a modified Jakob number, defined as

$$Ja = \left(\frac{\rho_f}{\rho_g}\right)^{1/2} \frac{C_{pl}(T_s - T_f)}{i_{fg}}. \tag{5}$$

Tien [4] proposed a similar correlation based upon the Kutateladze number, and pointed out that the flooding curve with this correlation exhibits a minimum point in the (K_g, K_f) plane. The unstable positive-slope portion results in a hysteresis effect. Nevertheless, the basic mechanism, as well as the necessary conditions for this effect, is not yet resolved.

EXPERIMENTAL

Apparatus

The experimental apparatus consists of a test section, steam supply line and circulating water loop, as shown in Fig. 1. The test section is made up of an upper and a lower chamber and a 1.3 m long square duct with a 9.5 × 9.5 cm cross-section. It has a support system which permits any inclination between 0° and 90°. For these data the angle of inclination with the horizontal was 4.0°. Water is introduced through a porous plate at the top portion of the test section and is drained at the lower chamber. During the partial delivery stage, part of the water entrained or carried upwards by the vapor flow is collected in the upper chamber. Hot water discharged from the test section is collected in a holding tank whose water level is controlled by a bypass solenoid control valve. The water inlet temperature can be regulated over the range 7–98 °C by varying the coolant rate to the heat exchanger. The steam comes from the building supply, which is nominally saturated and at a pressure of 1.02 MPa. When the steam enters the test section, it is superheated by 10–40 °C at atmospheric pressure.

Steam flow rates were measured with either 31.8 or 50.8 mm diameter venturis. The steam flow rate was calculated from the equation of state and the isentropic energy equation, based upon the measurements of thermodynamic state and pressure drop at the venturi. Agreement with the calibrated flow rate within an accuracy of ± 2% was obtained. The steam and water temperatures were measured with chromel–alumel thermocouples at the inlet and outlet of the test section. The calibration of the thermocouples showed agreement within ± 1 °C. The signals from

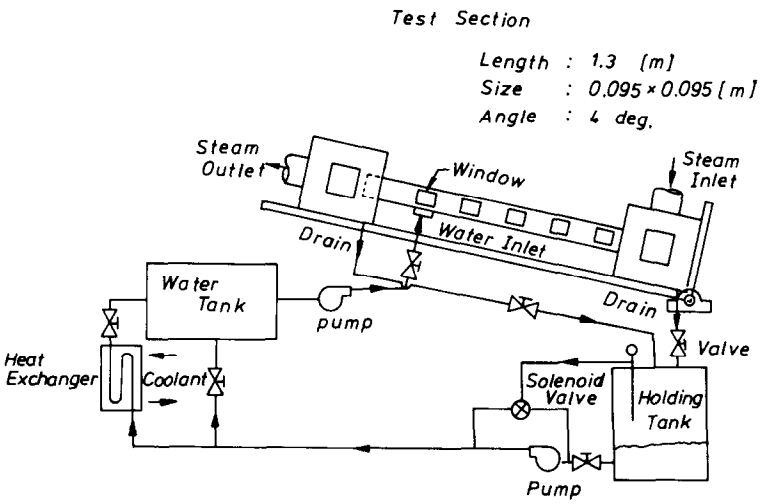

FIG. 1. Schematic diagram of experimental apparatus.

the thermocouples, transducers, and flowmeters were processed by a PDP 11-34 computer interfaced with a 16-channel AR-11 A/D converter. This computer-based data acquisition system has a maximum scan rate of approximately 30 kHz and a maximum scan repeat rate of 250 Hz. More details on the instruments are found elsewhere [8].

Procedures

The data on the onset of flooding in countercurrent steam-saturated water flow were obtained by either increasing or decreasing the steam flow rate at fixed water flow rates (water-first mode), or increasing the water flow rate at fixed steam flow rates (steam-first mode). In steam/subcooled water flow, however, the water-first mode (increasing steam flow) was used because the method of operation turned out to be unimportant, as will be seen later. The onset of flooding was determined mainly by visual observation, but occasional checks by means of pressure drop measurements were made to assure the reliability of the data [7]. In order to investigate the hysteresis effects, water penetration rates during the partial delivery stage were measured as a function of the upward steam flow rate at fixed water inlet flow rates. The penetration rate was obtained by measuring the level rise rate of water in the upper chamber. Since flow during the partial delivery stage is highly transient and oscillatory, effluent water was collected over a relatively long period in order to smooth out the fluctuations.

RESULTS AND DISCUSSION

Onset of flooding

A plot of the dimensionless vapor and liquid inlet volumetric flux in a non-condensing (steam/saturated water) flow at the onset of flooding and the recovery from flooding is shown in Fig. 2. The flooding velocities determined in the water-first mode are very similar to those in the steam-first mode, whereas the de-flooding points, which refer to the recovery points to a stable countercurrent flow as the steam flow rate is gradually decreased, lie slightly lower than the flooding points. A similar, but more pronounced, effect was also observed by Clift *et al.* [1] in a vertical single channel flow and by Liu *et al.* [15] in a vertical multiple path flow, possibly due to the absence of gravity as a stabilizing force on the liquid film. It appears, therefore, that the incipient flooding velocity is relatively insensitive to the method of operation in nearly-horizontal countercurrent flow.

As shown in Fig. 2, it is found that the locus of the onset of flooding jumps from the bottom of the test section to the top of the liquid injection rate when $J^*_{mf,\,in}$ increases above 0.094, resulting in different slopes for the flooding curve. This transition has also been found for a vertical annular air–water flow [16]. This appears to be associated with the presence of a hydraulic jump at the liquid entrance, which is pronounced at high liquid flow rates. At low flows flooding was initiated at the bottom of the present test section only after well-developed roll-waves had appeared on the interface. A rough thick liquid film was then observed with the formation of a water slug, whose crest height was several times the mean film thickness. At the onset of flooding, the water slug propagated backwards, carrying some liquid upwards over the entrance. Therefore, flooding may be regarded, in this region, as a limiting condition for countercurrent flow, which is retarded mainly by interfacial drag [8]. The effect of entrance and exit conditions in this region is thought to be relatively small. However, at high liquid injection rates ($J^*_{mf,\,in} > 0.094$), a stationary liquid slug appeared at the liquid entrance due to the hydraulic jump. The onset of flooding took place at the top as a result of

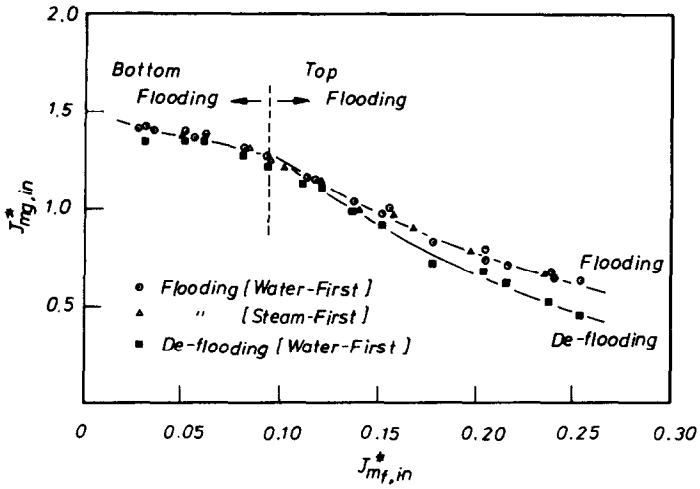

FIG. 2. Comparison of the flooding and de-flooding velocity in steam/saturated water flow.

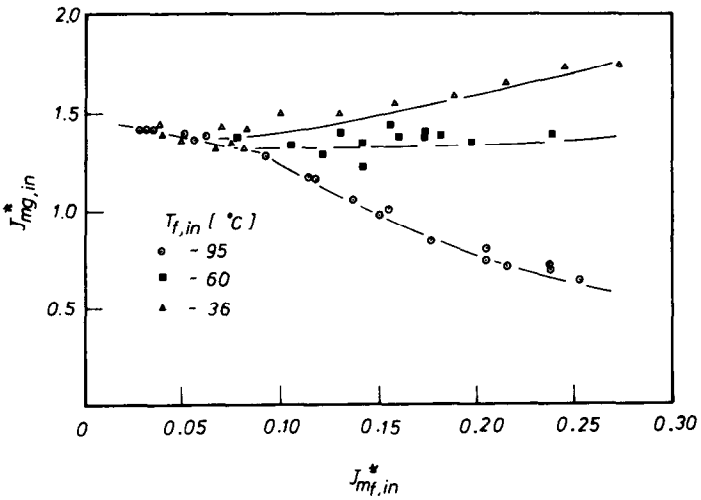

FIG. 3. Effect of the liquid inlet temperature on the onset of flooding in steam/subcooled water flow.

shearing off the crest of this slug. As the liquid injection rate was increased the slug height also grew, resulting in a considerable reduction of the vapor flooding velocity, compared to that for bottom flooding. In this region the initiation mechanism is basically governed by the liquid entrance condition.

Vapor flooding velocities in steam/subcooled water flow are illustrated in Fig. 3. The dimensionless liquid velocity for the transition to top flooding is slightly reduced as the initial subcooling becomes higher, owing to increased condensation. It is seen that larger steam supply rates are needed to initiate flooding at higher liquid subcoolings in the top-flooding regime. The difference between non-condensing and condensing flooding curves corresponds to the amount of steam condensed inside the test section. It should be pointed out that, for condensing flow, the liquid flow may exhibit locally a very chaotic flow pattern with the formation of a water slug at the bottom before flooding is initiated. However, this slug cannot propagate backwards to cause flooding due to the considerable loss of vapor momentum by condensation, as contrasted to non-condensing adiabatic flows. This result implies that the onset of flooding in the top-flooding regime occurs when the steam velocity at the liquid entrance reaches the non-condensing flooding velocity for a given liquid injection rate. Therefore, the global effect of condensation is important in determining the vapor flooding velocity in these cases. However, for bottom flooding this effect may be insignificant, as shown in Fig. 4. A comparison between the dimensionless vapor inlet and outlet velocity is shown in this figure as a function of the liquid subcooling for both top and bottom flooding. For top flooding ($J^*_{mf,in} = 0.190$), the vapor outlet velocity at the onset of flooding is almost constant,

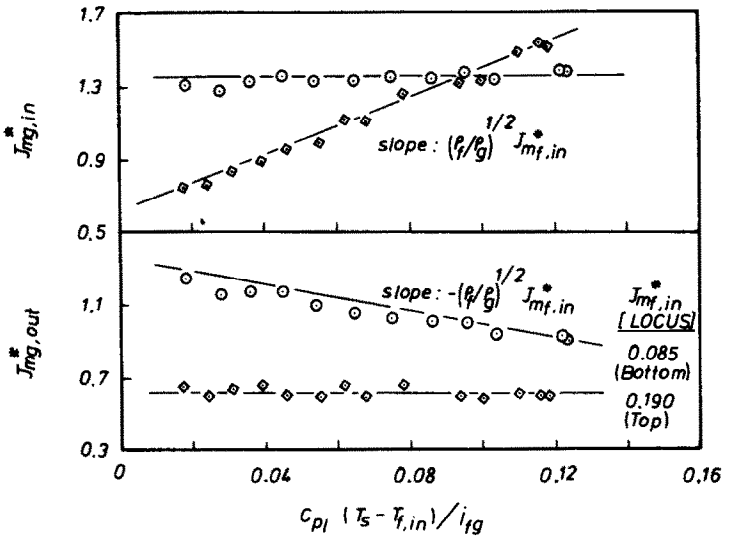

FIG. 4. Dimensionless inlet and outlet flooding velocities of top and bottom flooding with variation of the liquid subcooling.

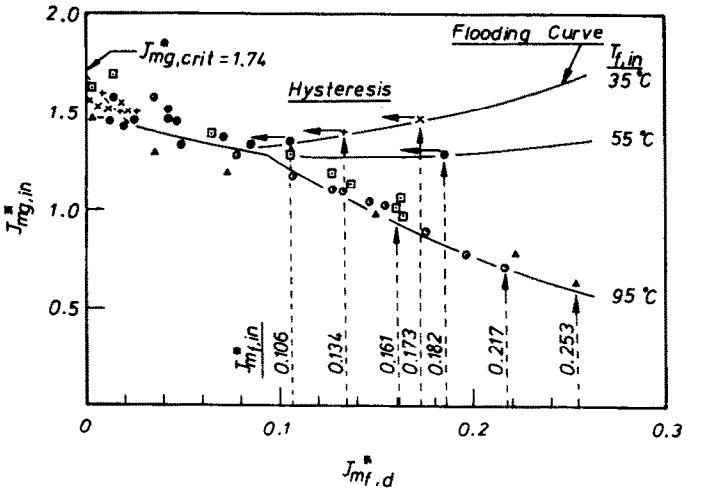

FIG. 5. Hysteresis effects during partial delivery stage.

regardless of the amount of liquid subcooling, whereas for bottom flooding ($J^*_{mf,in} = 0.085$) the vapor inlet velocity is likewise nearly constant. This result shows that the effective steam flow rate corresponds to the steam outlet flow rate for top flooding, and to the steam inlet flow rate for bottom flooding.

Hysteresis effects

There is often a sudden reduction of the liquid delivery rate immediately after flooding is initiated in countercurrent two-phase flow, due either to condensation or to the breakup of a liquid film. To study the mechanism of this effect, the liquid penetration rate for both saturated and subcooled inlet water was measured at various liquid flow rates, as shown in Fig. 5. One notes that the hysteresis effect appears only with subcooled water. The following mechanism for this hysteresis effect is proposed. At the onset of flooding a portion of the liquid phase is carried upwards by the steam flow and thus the downward liquid flow rate is reduced. This, in turn, decreases the overall condensation rate, resulting in a subsequent increase of the effective steam flow rate. This process now repeats rapidly until a stable partial delivery state is reached. The hysteresis observed in a vertical annular condensing flow by Liu and Collier [17] seems to occur with this mechanism. One can thus expect the hysteresis effect always to occur if flooding is initiated at the top of the tube in a condensing flow. On the other hand, hysteresis may also exist due to the breakup of a liquid film in an adiabatic countercurrent flow. Examples may be found in Clift *et al.* [1] and Wallis *et al.* [2]. The mechanism of this hysteresis should be distinguished from the one described earlier because no condensation is involved. Suppose that a liquid film is flowing downwards with

countercurrent gas flow. In order to attain the onset of flooding, the gas velocities must be fairly large, since the momentum exchange between the liquid and the gas phase is effected only by means of the interfacial shear if film flow is strictly maintained. However, if the liquid flow changes to the form of droplets with countercurrent gas flow, much smaller velocities are required to carry them upwards. When the flooding point is approached in countercurrent two-phase flow, a very rough liquid film with large-amplitude waves is developed. The crests of these waves are easily sheared off by the upward gas flow, resulting in considerable entrainment of liquid droplets. It is obvious that the gas momentum at the onset of flooding is large enough to lift these droplets past the liquid entrance. Therefore, if the liquid film is broken abruptly at the onset of flooding, a sudden reduction of the liquid delivery rate is also expected, leading to a hysteresis effect. However, the occurrence of this phenomenon seems to be dependent upon the entrance and exit conditions of the liquid. In the present test section, if flooding is initiated at the top as a result of the quasi-steady growth of a stationary liquid slug at the liquid entrance a continuous reduction of the delivery rate is obtained as the vapor velocity is increased beyond the flooding point. Therefore, a hysteresis effect due to the sudden disintegration of the liquid film at the hydraulic jump does not occur in the present tests, with a smooth entrance condition. Thus, the data points of the liquid delivery rate in non-condensing flow lie on the flooding curve, as shown in Fig. 5. This may also account for the nonexistence of the hysteresis effect in the vertical adiabatic countercurrent flow studied by Dukler and Smith [6]. It appears, therefore, that the occurrence of the hysteresis effect depends largely upon the locus of the onset of flooding.

Critical vapor velocity

The critical vapor velocity, by which we mean the gas velocity at the inception of a hanging film, was measured in condensing and non-condensing flows (Fig. 6). It is seen that the critical vapor velocity is independent of both the liquid injection rate and the initial liquid subcooling in nearly-horizontal countercurrent flow. The independence of the critical gas velocity of the liquid injection rate has been found also for a vertical adiabatic countercurrent flow [18, 19]. It is not surprising that the effect of condensation on the critical vapor velocity is insignificant. From Fig. 5, one notes that the data points of condensing flow exist only in the range of low liquid delivery rates, due to the hysteresis effects, and the two sets of data points in condensing and non-condensing flow converge as the delivery is decreased. Actually, the amount of condensation would be insignificant due to the small liquid delivery rate in this region. At the inception of a hanging film, all liquid is carried upwards over the liquid entrance by the vapor flow. The temperature of the liquid film is thus saturated, regardless of the initial liquid subcooling, and the critical vapor velocity is independent of the liquid subcooling, as the data indicate.

Countercurrent flow regime map

A countercurrent flow regime map in nearly-horizontal steam–water flow has been constructed, as shown in Fig. 7. Four distinct boundaries are indicated in the figure: 100% penetration line (Boundary A), the line of transition to a slug flow (Boundary B), zero penetration line (Boundary C), and the line of transition to a complete upward cocurrent flow (Boundary D). Below the flooding curve (Boundary A), a stable countercurrent stratified flow was maintained, although the interface exhibited various wave patterns, such as smooth, two- and three-dimensional wave, and roll-wave. The roll-waves superimposed on the three-dimensional waves, however, appeared only in the bottom-flooding region. The region between Boundaries A and B in the bottom-flooding region represents the growth of a water slug and the propagation of this slug backwards, which may be described as a preliminary stage on the onset of flooding [7]. In top-flooding cases, this region exhibited a stable partial delivery of the liquid with no significant change of the interfacial wave pattern. Beyond Boundary B, an oscillatory and transient plug flow developed with intermittent partial delivery, which could be observed also beyond Boundary A in the bottom-flooding cases. At Boundary C ($J^*_{mg,\,in} = 1.74$), a hanging film with an attachment point at the tube bottom appeared and the net delivery rate became zero. Between Boundaries C and D, an oscillatory hanging film was observed with the attachment point moving upwards as the steam flow rate increased. Finally, when the attachment point reached the liquid entrance, a completely cocurrent upwards steam–water flow developed, with a dry tube below the entrance. This transition took place at $J^*_{mg,\,in} = 2.05$, independently of the liquid injection rate and the initial subcooling. In condensation flow, only Boundary A (the flooding curve of the top-flooding region) moves upwards in the map owing to the global effect on condensation, as described earlier.

CONCLUDING REMARKS

A countercurrent flow regime map is developed which shows various flooding transitions in a nearly-horizontal stratified steam–water flow, such as the 0 and 100% liquid penetration lines and the transitions to slug flow and cocurrent upward flow. The influence of condensation on these transitions has been investigated, indicating that only the 100% liquid penetration line moves substantially upwards in the (J^*_{mf}, J^*_{mg}) plane due to the top-flooding effect. The critical vapor velocity is independent of the initial liquid subcooling as well as the inlet liquid flow rate.

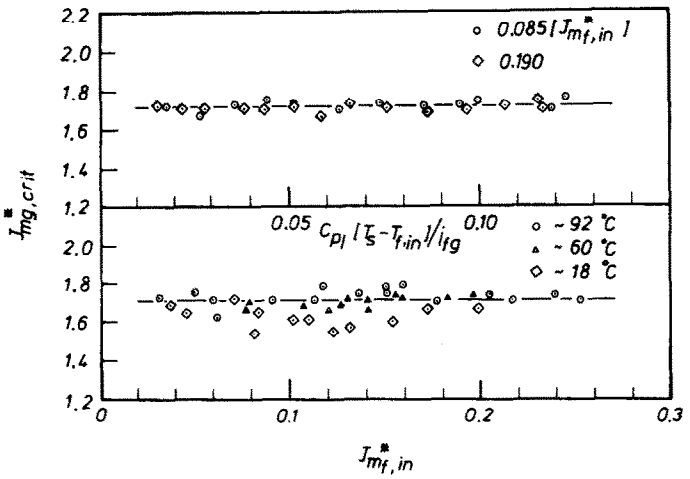

FIG. 6. Critical vapor velocity as a function of the liquid subcooling and liquid injection rate.

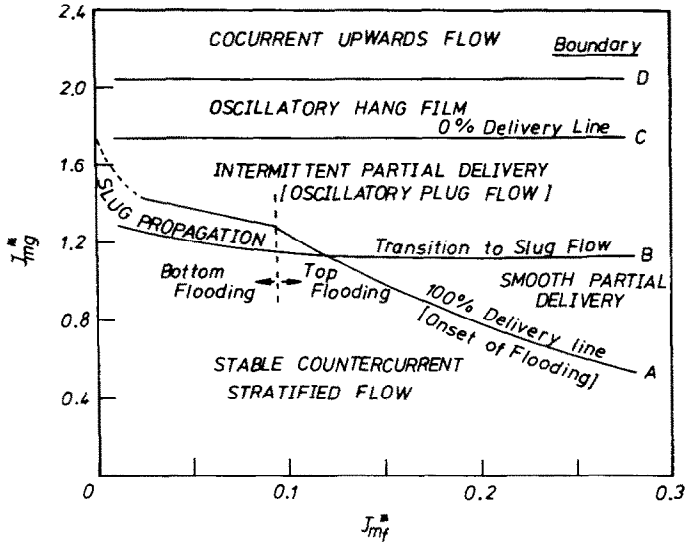

FIG. 7. Countercurrent flow regime map for nearly-horizontal steam/saturated water flow.

The onset of flooding takes place either at the liquid exit (bottom flooding) or at the liquid entrance (top flooding), depending upon the liquid injection rate. For bottom flooding, the global effect of condensation seems to be insignificant; however, condensation should be considered in calculating the vapor flooding velocity for top flooding. The global effect of condensation in top flooding also gives rise to a hysteresis effect during the partial delivery stage. The basic mechanisms of this effect have been described, based upon visual observations. Hysteresis due to the breakup of the liquid film has not been observed in the present study. This effect appears to take place when the onset of flooding is initiated at the liquid exit. The basic mechanisms of the hysteresis effects described in the present paper may provide a better understanding of the flooding phenomenon, and also help to resolve the contradictory experimental results on the existence of these effects.

REFERENCES

1. R. Clift, C. L. Pritchard and R. M. Nedderman, The effect of viscosity on the flooding conditions in wetted wall columns, *Chem. Engng Sci.* **21**, 87–95 (1966).
2. G. B. Wallis, D. C. de Sieyes, R. J. Roselli and J. Cacombe, Countercurrent annular flow regimes for steam and subcooled water in a vertical tube. EPRI Report, NP-1336 (1980).
3. G. B. Wallis, Flooding velocities for air and water in vertical tubes, UKAEA Report, AAEW-R123 (1961).
4. C. L. Tien, A simple analytical model for countercurrent flow limiting phenomena with condensation, *Lett. Heat Mass Transfer* **4**, 231–237 (1977).
5. G. F. Hewitt, Influence of end conditions. Tube inclination and physical properties on flooding in gas–liquid flows, Harwell Report, HTFS-RS222 (1977).
6. A. E. Dukler and L. Smith, Two-phase interactions in countercurrent flow: studies of the flooding mechanism, NUREG/CR-0617 (1979).
7. S. C. Lee and S. G. Bankoff, Stability of steam–water countercurrent flow in an inclined channel: flooding, *J. Heat Transfer* **105**, 713–718 (1983).

8. S. C. Lee and S. G. Bankoff, Parametric effects on the onset of flooding in flat-plate geometries, *Int. J. Heat Mass Transfer* **27**, 1691–1700 (1984).
9. G. B. Wallis and J. E. Dobson, The onset of slugging in horizontal stratified air–water flow, *Int. J. Multiphase Flow* **1**, 173–193 (1973).
10. K. Mishima and M. Ishii, Theoretical prediction of onset of horizontal slug flow, *J. Fluids Engng* **102**, 441–445 (1980).
11. E. S. Kordyban and T. Ranov, Mechanism of slug formation in horizontal two phase flow, *Am. Soc. Mech. Engrs, J. Basic Engng* **92**, 857–864 (1970).
12. S. G. Bankoff and S. C. Lee, A comparison of flooding models for air–water and steam–water flow, *Advances in Two-phase Flow and Heat Transfer*, NATO AS1 Series, No. 64, Vol. 2. pp. 745–780. Martinus Nijhoff, The Hague, The Netherlands (1983).
13. K. S. Chung, L. P. Liu and C. L. Tien, Flooding in two-phase countercurrent flows—II. Experimental investigation, *Physicochemical Hydrodynamics* **1**, 209–220 (1980).
14. J. A. Block and C. J. Crowley, Effect of steam upflow and superheated walls on ECC delivery in a simulated multiloop PWR geometry, Creare Report TN-210 (1976).
15. C. P. Liu, G. E. McCarthy and C. L. Tien, Flooding in vertical gas–liquid countercurrent flow through multiple short paths, *Int. J. Heat Mass Transfer* **25**, 1301–1312 (1982).
16. G. L. Shires and A. R. Pickering, The flooding phenomenon in countercurrent two-phase flow, *Proc. Symp. Two-phase Flow*, University of Exeter, England, Vol. 2, pp. B501–B538 (1965).
17. J. S. K. Liu and R. P. Collier, Heat transfer in vertical countercurrent steam–water flooding flows, *Basic Mechanisms in Two-phase Flow and Heat Transfer*. ASME, New York (1980).
18. G. B. Wallis and S. Makkencherry, The hanging film phenomenon in vertical annular two-phase flow, *J. Fluids Engng* **96**, 297–298 (1974).
19. O. L. Pushkina and U. L. Sorokin, Breakdown of liquid film motion in vertical tubes, *Heat Transfer—Soviet Res.* **1**, 56–64 (1969).

ENGORGEMENT ET EFFETS D'HYSTERESE DANS UN ECOULEMENT PRESQUE HORIZONTAL, STRATIFIE DE VAPEUR D'EAU A CONTRE-COURANT

Résumé—On présente des résultats expérimentaux sur les transitions d'engorgement et avec un régime d'écoulement à contre-courant presque horizontal ($\theta = 4$), stratifié de vapeur et d'eau. On explore l'influence de la condensation sur les mécanismes d'apparition de l'engorgement. On étudie le mécanisme des effets d'hystérèse, lié à la condensation, qui sont observés pendant le stage de libération partielle dans un écoulement vapeur/eau sous-refroidie.

"FLOODING" UND HYSTERESE-ERSCHEINUNGEN IN EINER FAST-WAAGERECHTEN, GEGENLÄUFIGEN, GESCHICHTETEN STRÖMUNG VON WASSERDAMPF UND FLÜSSIGEM WASSER

Zusammenfassung—Es werden Versuchsergebnisse bezüglich der Übergangserscheinungen beim "Flooding" vorgelegt—zusammen mit einer Strömungsbilderkarte für die fast-waagerechte ($\theta = 4{,}0$), gegenläufige, geschichtete Strömung von Wasserdampf und flüssigem Wasser. Der Einfluß der Kondensation auf das Einsetzen und die grundlegenden Mechanismen des "Flooding" werden untersucht, ebenso die Mechanismen der Hysterese-Erscheinungen infolge der Kondensation, welche während der teilweisen Förderung in einer Strömung aus Wasserdampf und unterkühltem Wasser beobachtet werden.

ЭФФЕКТЫ ЗАТОПЛЕНИЯ И ГИСТЕРЕЗИСА В ПОЧТИ ГОРИЗОНТАЛЬНОМ ПРОТИВОТОЧНОМ СТРАТИФИЦИРОВАННОМ ПАРОВОДЯНОМ ПОТОКЕ

Аннотация—Представлены экспериментальные данные по эффектам затопления, а также карты противоточного режима течения для почти горизонтального ($\theta = 4{,}0$) стратифицированного паровоДяного потока. Исследованы влияние конденсации на возникновение и основные механизмы затопления и гистерезиса, вызванные конденсацией.